

**Fig. 2.** General synthesis route and structure of ASA. R1 and R2 are alkyl chains.

With reference to Figs. 1 and 2, it should be noted that the detailed structures of commercial AKD and ASA vary according to the used olefin chain compositions (e.g. length, typically C<sub>14</sub>-C<sub>20</sub>, and branching).

AKD and ASA are extensively used in papermaking as sizing agents (Gess 1992; Neimo 1999). These so-called reactive sizes were first introduced already in the 1950s (Davis et al. 1956) and 1960s (Wurzberg and Mazzarella 1963). Yet, they were not very widely applied before the increased use of calcium carbonate and trend towards alkaline papermaking during the last two decades. Currently they are used to confer hydrophobicity to cellulose fibres in neutral and alkaline papermaking. Various features, related to their use in papermaking process, have been studied. These include e.g. adhesion forces between AKD and cellulose (Bogdanovic et al. 2001), adhesion properties of ASA sized paper surfaces (Dickson and Berg 2001), wetting dynamics of AKD on cellulosic surfaces (Garnier et al. 1999), spreading and adhesion of ASA on different surfaces (Lindfors et al. 2005a; Lindfors et al. 2005b), and many aspects of emulsion stability and sizing efficiency (Asakura et al. 2006; Hodgson 1994; Isogai et al. 1992a; Isogai et al. 1992b; Isogai et al. 1994; Isogai et al. 2004; Taniguchi et al. 1993). Nonetheless, more detailed knowledge of chemical interactions, and phenomena such as adhesion and adsorption, is still needed to be able to better master the use of AKD and ASA, to formulate more stable emulsions, to optimize the sizing result, and to avoid contamination. In the study of basic chemical interactions, model surfaces are essential. It is noteworthy that in spite of numerous studies, there is still a lack of controlled model surfaces prepared from AKD and ASA. Such model surfaces can contribute to further investigation of e.g. formation of stabilizing polyelectrolyte layers in size emulsification, interactions of sizing agents with cellulose and other materials present in papermaking stock, and adhesion forces leading to contamination of paper machines.

The aim of this study was to establish simple methods for preparing well-defined AKD and ASA model surfaces for fundamental studies of adhesion interactions. Surfaces prepared here are not intended to simulate paper sizing as such. In addition, adhesion force measurements with atomic force microscopy (AFM) and through contact angle measurements were performed in order to demonstrate the applicability of the created surfaces to these measurements.

## EXPERIMENTAL

### Materials

A commercial Alkyl Ketene Dimer (AKD) with a melting point above 60°C, from Kemira Oyj, Vaasa, Finland, was used for all AKD model surfaces. The AKD was purified by recrystallizing it twice from acetone. Recrystallized AKD was used in all experiments. Alkenyl Succinic Anhydride (ASA) surfaces were prepared from a wax, which was solid at room temperature. The ASA was supplied by Kemira Chemie GmbH, Krems, Austria. The original purity, before recrystallization, of both AKD and ASA was > 95 % (according to the supplier). Impurities were mainly residual olefin chains from the synthesis. Untreated smooth silicon wafers (Okmetik Oy, Helsinki, Finland) and QCM-D gold crystals (Q-Sense AB, Gothenburg, Sweden) were used as substrates for the AKD and ASA films. Glass spheres (Whitehouse Scientific Ltd., UK) were used for colloidal probe measurements. All other chemicals used were of analytical grade and Milli-Q water was used throughout the investigation.

### Surface Preparation

#### *Casting*

Sodium chloride IR crystal windows from Sigma-Aldrich were used for casting AKD and ASA surfaces from molten wax (method earlier described by Zbik et al. (2006)).

#### *Spin-coating*

A Laurel Technologies Corporation WS-400B-6NPP/LITE spin-coater (Laurell Technologies Corp., USA) was used. Spin-coating time was 60 s, AKD and ASA solution concentration and spin-coating speed were varied to prepare films of different thicknesses.

### Surface Characterization and Adhesion Measurements

#### *Ellipsometry*

Angle resolved laser (632.8 nm) ellipsometry (Picoellipsometer, Beaglehole Instruments) was used to determine the thickness of the AKD and ASA films on SiO<sub>2</sub> substrates. The data were collected in 0.5 degree intervals from 68 to 80 degrees. The angles were chosen around the Brewster angle since the sensitivity for changes in the layer thickness is the highest close to this angle. The thicknesses of the AKD and ASA films were determined by fitting the measured data to a two-layer model. The optical properties of the silicon substrate were taken from the data bank of the fitting software (TFCompanion, Semiconsoft). AKD and ASA were considered as dielectric materials having a real index of refraction equal to 1.46 (Mischki et al. 2006).

#### *X-ray photoelectron spectroscopy, XPS*

An AXIS 165 electron spectrometer and monochromatic Al K $\alpha$  irradiation was used for acquisition of XPS spectra. Before analysis, all samples were pre-evacuated overnight in order to stabilize vacuum conditions. By parallel measurements on a reference sample (TKK reference sample (Johansson and Campbell 2004)), included with

each sample batch, it was verified that UHV conditions remained satisfactory and non-contaminating. No sample deterioration was detected during the experiment. All samples were analysed at three locations (analysis area ca. 1 mm<sup>2</sup>). Elemental surface compositions were determined from low-resolution scans recorded with 80 eV analyser pass energy and 1 eV step. Carbon and oxygen high resolution spectra were recorded from O 1s and C 1s regions using 20 eV analyser pass energy and 0.1 eV step.

#### *Atomic Force Microscopy, AFM*

AFM imaging was performed using a NanoScope IIIa Multimode scanning probe microscope (Digital Instruments, Inc. Santa Barbara, CA, USA). The surfaces were scanned in tapping mode in air using commercial Si cantilevers (Digital Instruments) with a resonance frequency of about 300 kHz. Four images were recorded for each surface and representative micrographs were chosen for presentation. Atomic force microscopy (Nanoscope IIIa) was also used to measure surface forces using the colloidal probe technique (Butt 1991; Ducker et al. 1991). Briefly, a glass sphere with diameter 31.3 µm was glued to the tipless end of a cantilever with a reported spring constant of 0.38 and 0.58 N/m (Veeco Instruments, Santa Barbara, CA, USA). Surface forces were measured against AKD and ASA surfaces in air and in 1 mM NaHCO<sub>3</sub>. The surface force was calculated from the deflection of the cantilever using Hooke's law in the conventional way and normalized by the radius of the glass spheres (Derjaguin 1934). The spring constants were determined by the reference spring method (Torii et al. 1996; Tortonese and Kirk 1997). For the sake of clarity, only one representative curve per system is shown in the figures. However, the actual values of the pull-off forces and the pressing loads may contain an error due to the nonlinearity of the AFM piezo scanner and the sliding of the colloidal probe (Stiernstedt et al. 2005).

#### *Contact angle measurements*

A CAM 200 contact angle goniometer (KSV Instruments Ltd, Helsinki, Finland) was used for determination of contact angles of water and diodomethane on the AKD and ASA model films in ambient air. The size of the water drops was ca. 10 µl and that of diodomethane drops ca. 3 µl. Contact angles were calculated by Axisymmetric Drop Shape Analysis (ADSA) using software delivered with the instrument. This analysis is based on fitting experimentally determined drop profiles to the full equations for drop profiles of sessile drops under the influence of gravity derived from the Young-Laplace equation. The fitting method is based on the principle described by Jennings and Pallas (1988).

## RESULTS AND DISCUSSION

### **Surface Preparation**

Casting is an easy and fast method for creating fully covering surfaces from both AKD and ASA. However, melting the hydrophobic wax and letting it cool down in air results in a noticeably rough surface. To overcome this roughness, surfaces were cast against freshly cleaved sodium chloride crystals and the salt crystal was removed by

dissolution in water after letting the wax to cool down slowly at room temperature. Mirror-like surfaces of both AKD and ASA were achieved in this way. Zbik et al. have earlier used similar casting method in preparing paraffin wax surfaces (Zbik et al. 2006). Using a NaCl crystal resulted in significantly smoother surfaces than casting in air or against any smooth surface that had to be cleaved from the wax after casting.

Cast surfaces can be used e.g. for adhesion measurements using the colloidal probe technique and for contact angle measurements. These surfaces are also ideal for recording reference spectra using surface sensitive techniques such as XPS, because rather thick and fully covering layers are formed. However, many surface interaction measurement techniques do require thin or ultra-thin surfaces, which can be fast and feasibly created e.g. by spin-coating.

Model films of AKD and ASA were also prepared by spin-coating from different organic solvents on SiO<sub>2</sub> and gold substrates. AKD and ASA concentrations from 0.5 g/l to 50 g/l were applied, and toluene, n-hexane, ethanol, and acetone were used as solvents. Spin-coating speed was varied between 1000 rpm and 6000 rpm. Spin-coated layers from both toluene and n-hexane solutions were reasonably uniform in macroscopic scale. Films from toluene solutions were selected to be further investigated here, because of the good solubility of AKD and ASA in toluene and the low evaporation rate of this solvent. Microscopy images (magnifications of 5x, 20x, and 100x) of AKD and ASA layers on SiO<sub>2</sub> substrates spin-coated from 2.5 g/l toluene solution at a spin rate of 2700 rpm are shown in Figs. 3 and 4. The AKD surface (Fig. 3) appeared so smooth through the microscope that some scratches were made to the surface in order to introduce contrast to the image and to verify that there was an AKD layer on the SiO<sub>2</sub> substrate. On the ASA surface (Fig. 4) circles of 50 – 300 μm in diameter can be seen. The surface is not as smooth in macroscopic scale as that of AKD.

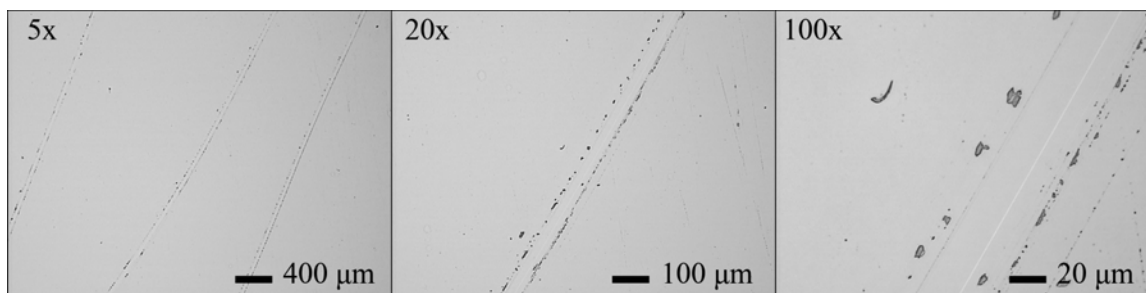


**Fig. 3.** Microscopy images of spin-coated AKD (2.5g/l in toluene, 2700 rpm) of different magnifications (5x, 20x, and 100X). Scratches on the surfaces are made to introduce some contrast to the image.

Patterning of ASA surfaces was observable regardless of the solvent used, spin-coating parameters, or ASA concentration. An example of clear patterning is shown in Fig. 5, where microscope images of ASA layer spin-coated on SiO<sub>2</sub> from 50 g/l toluene solution at a spin rate of 5000 rpm are shown. Based on thinner surface layers of ASA (Fig. 4) one might consider that incomplete wetting could cause the patterns. However, the thick surface (Fig. 5) indicates that, at least here, this is not the case. The patterns could rather be because of ASA molecule orientation.

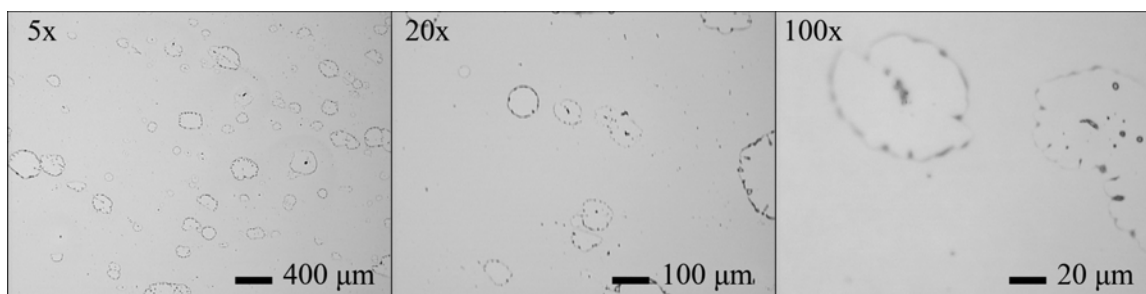


**Fig. 4.** Microscopic images of spin-coated ASA (2.5g/l in toluene, 2700 rpm) of different magnifications (5x, 20x, and 100X).

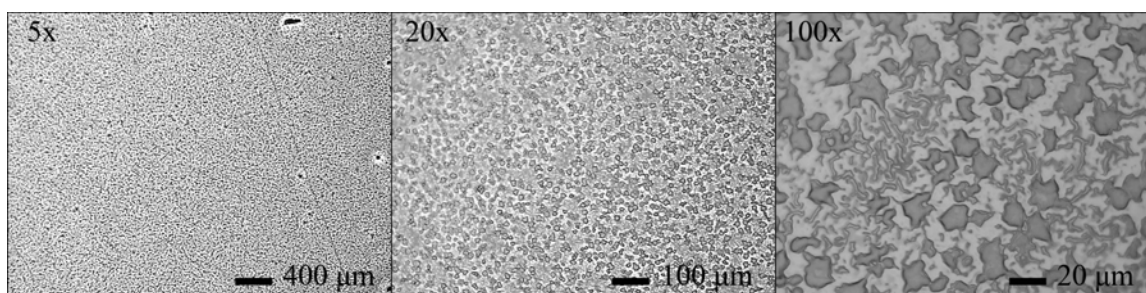


**Fig. 5.** Microscopic images of spin-coated ASA (50g/l in toluene, 5000 rpm) of different magnifications (5x, 20x, and 100X).

### Determination of AKD and ASA Film Thickness

The thickness of spin-coated AKD and ASA films was determined using ellipsometry. AKD layer thickness as a function of the AKD concentration of the spun toluene solution is shown in Fig. 6 (spin rate 5000 rpm).

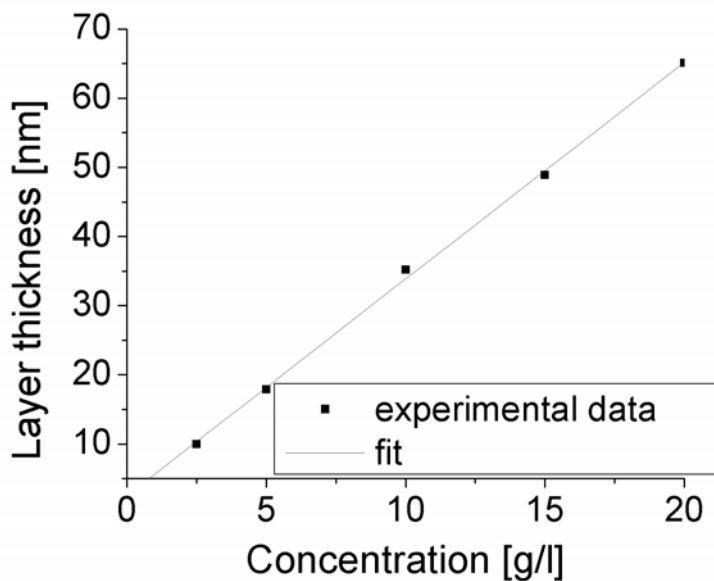


**Fig. 6.** Thickness of AKD model film vs. spin-coating solution conc. (spinning rate: 5000 rpm).

Similar data for ASA is presented in Fig. 7. The results show that films of varying thickness could be easily prepared by simply changing the concentration of the spin-coating solution. The same effect could also be reached by variations of spin rate; at constant concentration the layer is the thicker, the lower the speed of spinning. It is also obvious that layers created from AKD and ASA had very similar thicknesses when identical concentrations were used.

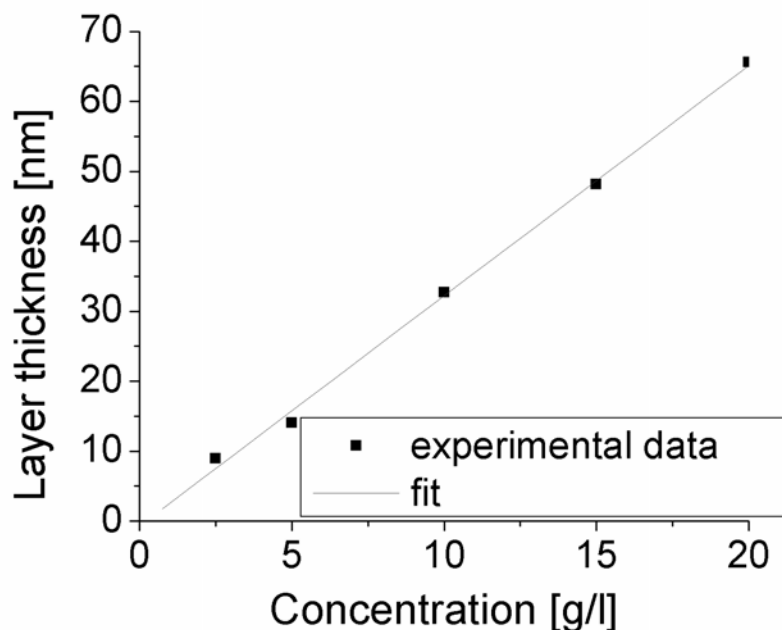


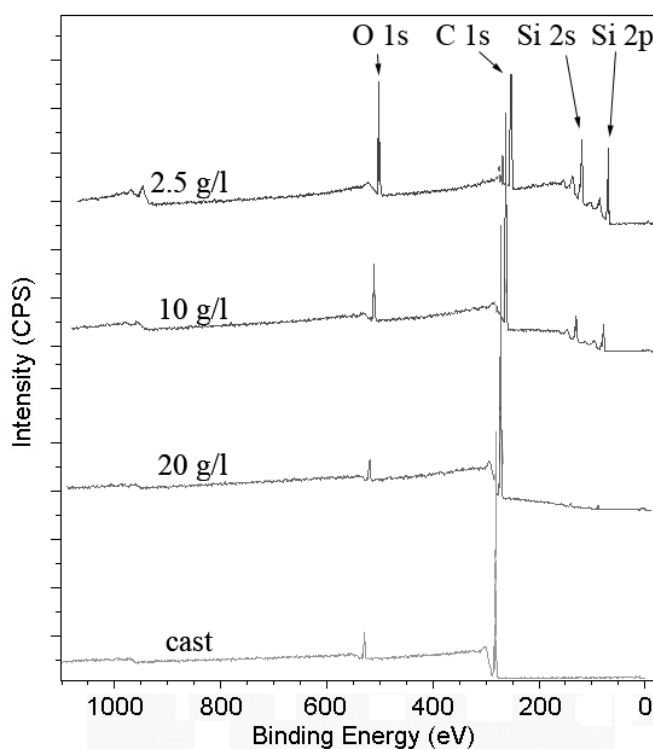
Fig. 7. Thickness of ASA model film vs. spin-coating solution conc. (spinning rate: 5000 rpm).

### Chemical Composition of the Model Surfaces

The elementary composition of the model surfaces of AKD and ASA was determined using XPS. The atomic ratios between oxygen and carbon, between silicon and carbon, and the relative amounts of different carbon peaks for AKD and ASA films spin-coated from 2.5 g/l, 10 g/l, and 20 g/l toluene solutions (at spin rate 5000 rpm), in addition to those of cast surfaces, are shown in Table 1. The thinnest surface layers (prepared from 2.5 g/l solution), which were found to be ca. 10 nm thick by ellipsometry, showed significant amounts of silicon and oxygen on the surface. Thus, these surface layers of AKD and ASA were obviously not fully covering, because the SiO<sub>2</sub> substrate was clearly detectable by XPS. Layers prepared from higher concentrations (10 g/l and 20 g/l) of AKD and ASA provided almost similar atomic ratios as the cast surfaces, and one can conclude that these concentrations were high enough to create a covering model surface from AKD and ASA. XPS spectra of different AKD layers are presented in Fig. 8 to visually demonstrate the effect of the layer thickness to the recorded spectrum. The most significant changes can be seen in the Si peaks at ca. 150 eV and 100 eV.

**Table 1.** O/C Atomic Ratio, Si/C Atomic Ratio and Relative Amounts of Different Carbons for the Model Surfaces

Material	O/C	Si/C	C1	C2	C3	C4
AKD, 2.5 g/l	0.32	0.45	37	47	3	1
AKD, 10 g/l	0.076	0.065	63	8	1	1
AKD, 20 g/l	0.045	0.015	76	5	2	1
AKD, cast	0.044	0.003	89	1	2	1
ASA, 2.5 g/l	0.32	0.29	75	17	-	7
ASA, 10 g/l	0.18	0.041	80	12	-	8
ASA, 20 g/l	0.17	0.034	80	13	-	7
ASA, cast	0.19	0.025	84	9	-	7

**Fig. 8.** XPS wide scan spectra of AKD. 2.5 g/l, 10 g/l, 20 g/l, and cast surface. The spectra are shift vertically for clarity.

### Surface Topography of AKD and ASA Films

An AFM topographic image of the AKD film cast against NaCl crystal is shown in Fig. 9. The rms value of the  $1 \mu\text{m}^2$  image area is 5.95 nm. However, there is a higher peak to the right on the image, which contributes substantially to the roughness, and the rms of the rather flat area to the left was determined to be 1.34 nm. Cast ASA surfaces showed a generally similar topography to the one shown here for AKD. Although cast surfaces were not completely flat, i.e. there occurred some larger roughness features (as that shown in Fig. 9), which were most likely due to uneven cleavage of NaCl crystals,

their rms values was well within the range that is appropriate for adhesion measurements by colloidal probe technique and contact angle measurements (e.g. Notley et al. have recently used cellulose spheres with similar surface roughness in colloidal probe microscopy measurements (Notley et al. 2006)).

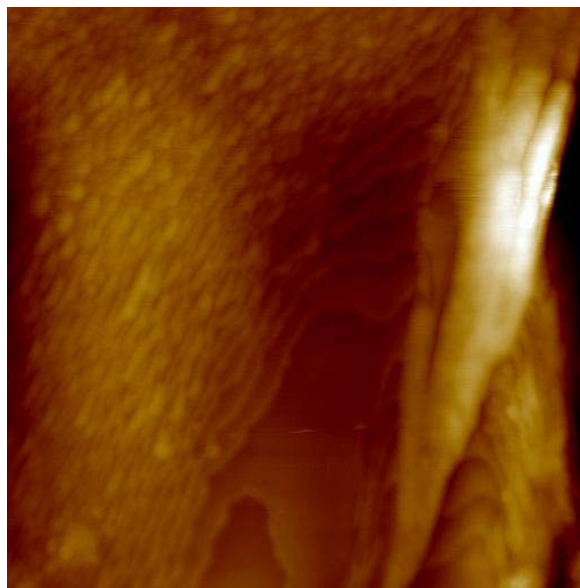


**Fig. 9.** AKD NaCl (1  $\mu\text{m}$ ,  $z = 45$  nm, rms = 5.95 nm/upper left corner 1.34nm).

Both macroscopic inspection and ellipsometry indicated that even the AKD and ASA layers spin-coated from the lower concentrations would be relatively smooth and covering. However, XPS analysis showed that full coverage was not reached. AFM imaging was used to further study these surfaces. A 25  $\mu\text{m}^2$  topography image of a spin-coated AKD film is presented in Fig. 10a and a 1  $\mu\text{m}^2$  image within the former image is shown in Fig. 10b. The surface was spin-coated on  $\text{SiO}_2$  from 2.5 g/l toluene solution. From the larger image it is clear that no uniform coating was reached, but a layered structure was formed. Individual layer steps can be more clearly seen in the 1  $\mu\text{m}^2$  image. The structure of spin-coated ASA films was very similar to that of AKD (see Fig. 11a,b). In Fig. 11b shows a step profile of the surface, indicating clearly the ca. 2.5 nm layers of ASA. Ren et al. (2004; 2003) have recently studied stearic acid, which has a C-18 carbon chain, and can thus be used as a reference for the ASA used here. The ASA monolayer thickness of  $\approx 2.5$  nm corresponds fairly well with the value of ca. 2 nm found for stearic acid. Apparently the deepest spots on the surfaces presented in Fig. 10a and 11a are not covered by AKD or ASA at all, so that the  $\text{SiO}_2$  substrate can still be seen. As the ellipsometry data showed, the surface thickness was  $\approx 10$  nm, while the AFM images indicate that the thickness of one molecular layer was  $\approx 2.5$  nm. Thus, it is obvious that an average four layers of AKD/ASA was deposited on the surface. The rms values of spin-coated AKD and ASA layers are generally acceptable for model surface purposes.

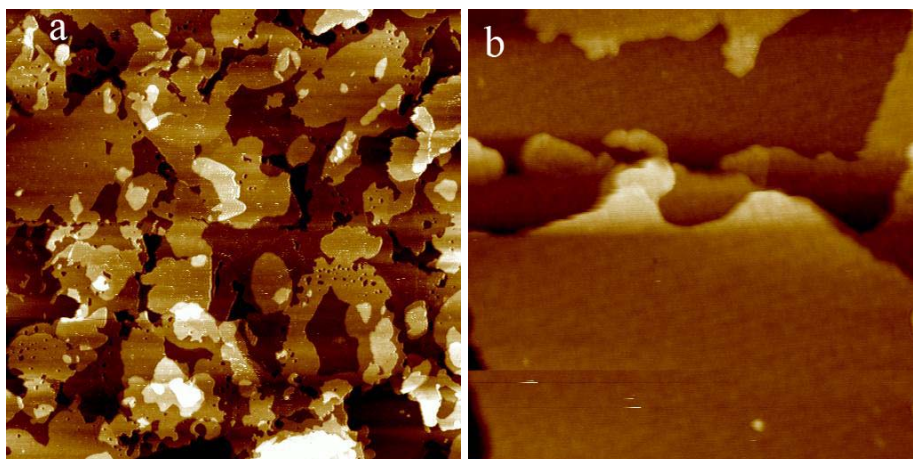


**Fig. 10.** Spin-coated (2.5 g/l, 2700 rpm) AKD on SiO<sub>2</sub> a) 5 μm, z = 14 nm, rms = 3.14 nm b) 1 μm, z = 14 nm, rms = 1.36 nm.

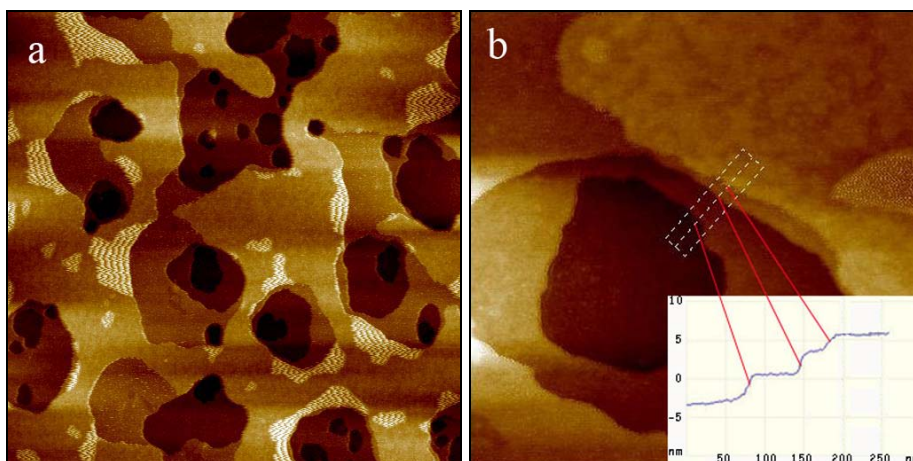


**Fig. 11.** Spin-coated (2.5 g/l, 2700 rpm) ASA on SiO<sub>2</sub> a) 5 μm, z = 18 nm, rms = 2.88 nm b) 1 μm, z = 15 nm, rms = 1.38 nm.

To check how the spin-coated layer followed the topography of the used substrate, a layer of AKD was spin-coated on gold. Fig. 12a shows an AFM image of the gold substrate and Fig. 12b an AKD film spin-coated on top of it. It can be seen that the topography of the substrate with spherical texture is well reproduced on the AKD surface. Also, the layered structure observed on AKD coated on SiO<sub>2</sub> can be seen and the rms roughness is of the same order of magnitude as on SiO<sub>2</sub>.

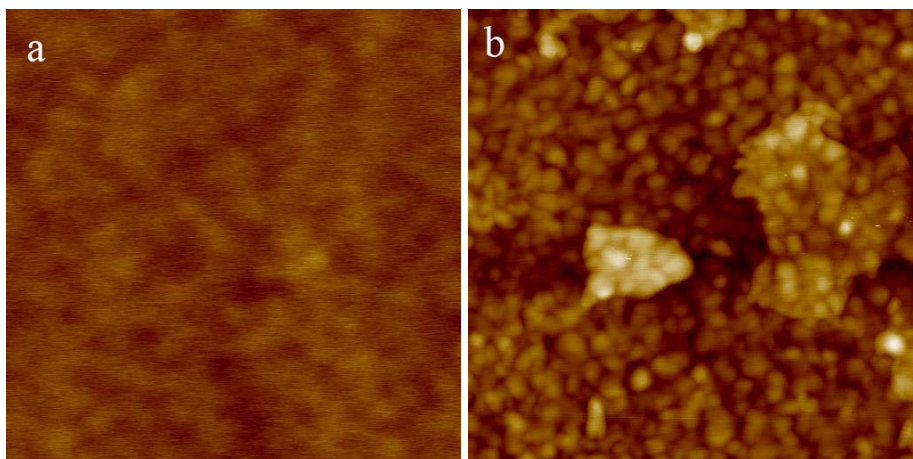


Fig. 12. a) Au b) AKD on Au (1  $\mu\text{m}$ ,  $z = 15 \text{ nm}$ ,  $\text{rms} = 1.46 \text{ nm}$ ).

### Water Contact Angles on AKD and ASA Surfaces and the Surface Stability

Contact angles of water on AKD surfaces prepared by casting and spin-coating are presented in Fig. 13. It can be seen that even the thinner (not fully covering) AKD film was clearly more hydrophobic than the  $\text{SiO}_2$  substrate. The contact angles of water on the cast and the thicker spin-coated surface were nearly equal. This supports the finding that a concentration of 10 g/l was roughly sufficient to spin-coat a covering AKD layer. The contact angle on the thinner AKD surface was not as high as on the thicker surfaces, which must be due the contribution of the more hydrophilic  $\text{SiO}_2$  spots to the overall contact angle. The contact angle data recorded on each of the AKD surfaces showed good stability of the surfaces (the contact angle remained stable after a very short equilibration period).

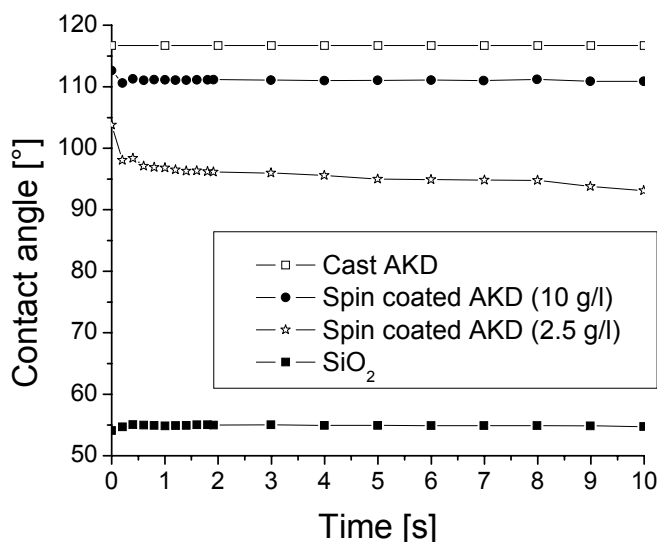
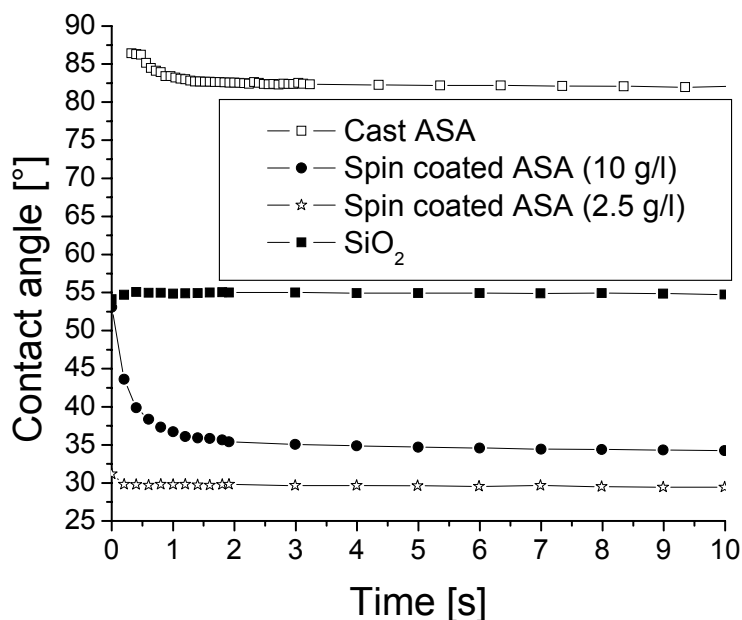


Fig. 13. Contact angle of water on AKD surfaces prepared by casting and spin-coating, and on the  $\text{SiO}_2$  substrate.

Contact angles of water on ASA surfaces are presented in Fig. 14. These follow a rather different trend from the one observed with AKD; water spreads fairly fast on thin ASA layers, and a thick cast film was needed to create a hydrophobic surface. In fact, a smaller contact angle was obtained on these spin-coated ASA layers than on the  $\text{SiO}_2$  substrate. We believe that this is associated with the reactivity of ASA (hydrolysis reactions of spin-coated ASA layer with water droplet on it). The reaction products of hydrolysed ASA are probably highly surface active and reduce the water contact angle to an even lower level than that of pure water on  $\text{SiO}_2$ . Figure 15 shows water contact angles recorded on a thicker spin-coated ASA surface. This surface was prepared from a 50 g/l concentration and the layer thickness was determined to be ca. 200 nm. A clear drop in contact angle was observed after ca. 90 s. This indicates that even a rather thick spin-coated layer of ASA on  $\text{SiO}_2$  is unstable in presence of water. These measurements performed on ASA layers of different thickness indicate that it might be possible to e.g. assess the hydrolysis rate issues through a set of similar measurements with several different ASA layer thicknesses.

Contact angles of diiodomethane (which is not reactive towards ASA like water) on ASA surfaces were recorded to verify that the observations of water spreading on the ASA films was really due to the hydrolysis reactions. Diiodomethane contact angles are presented in Fig. 16. Relatively similar spreading kinetics was observed both on the ultrathin (ca. 10 nm) ASA film and on the thick cast ASA layer. This indicates that when there is no reactivity between the probing liquid and the model surface the layer thickness does not affect the spreading of the liquid. This result further supports the conclusion that ASA reactivity caused the instability of the ASA layers in contact with water.



**Fig. 14.** Contact angle of water on ASA surfaces prepared by casting and spin-coating, and on the  $\text{SiO}_2$  substrate.

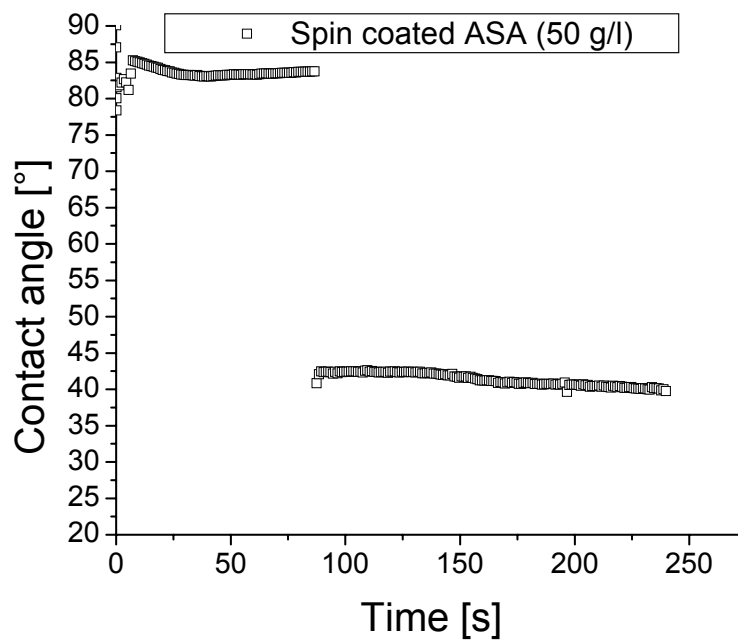


Fig. 15. Contact angle of water on a ca. 200 nm ASA surface prepared by spin-coating.

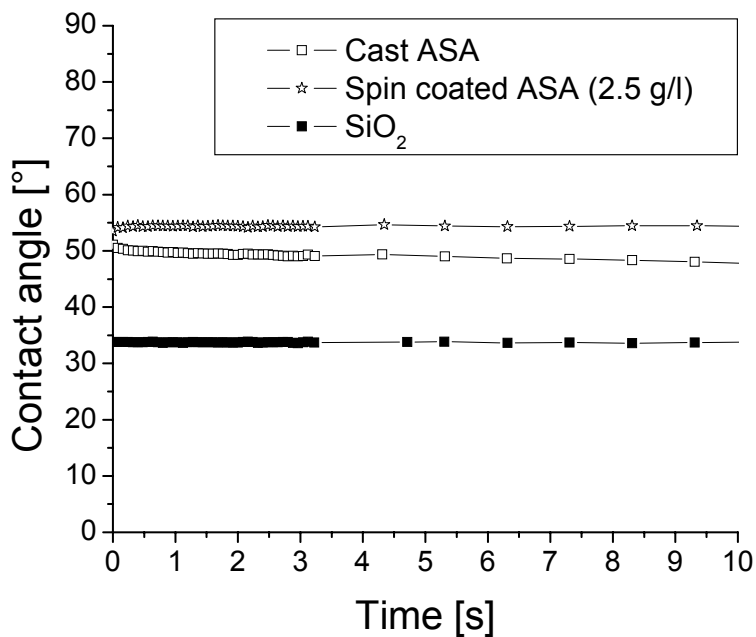


Fig. 16. Contact angle of diodomethane on ASA surfaces prepared by casting and spin-coating, and on the SiO<sub>2</sub> substrate.

## Adhesion of AKD and ASA

The suitability of the created model surfaces for adhesion studies was demonstrated by contact angle and colloidal probe experiments. Measurements of adhesion, utilizing spin-coated AKD and ASA surfaces, have also been done using a contact mechanics measurement technique, and are presented elsewhere (Lindfors et al. 2007).

Adhesion of ASA on hydrophilic and hydrophobic surfaces was evaluated earlier, using contact angle measurements (Lindfors et al. 2005b). These showed a discrepancy in the calculation of ASA contact angles on aqueous solutions, which we deemed to originate from the fact that the fast hydrolysis reactions occurring on the ASA/aqueous solution interface resulted in incorrect interfacial tension values. We have used the contact angles recorded here on a cast ASA surface to calculate ASA/water interfacial tension,  $\gamma_{ASA-water}$  from Young's equation:

$$\cos \theta = \frac{\gamma_{ASA-air} - \gamma_{ASA-water}}{\gamma_{air-water}} \quad (1)$$

where  $\theta$  denotes the contact angle of water on ASA and  $\gamma_{ASA-air}$ ,  $\gamma_{ASA-water}$  and  $\gamma_{air-water}$  are interfacial tensions. Assuming that earlier measured value of ASA surface tension in air (33.2 mJ/m<sup>2</sup>) is correct and using water surface tension 72.8 mJ/m<sup>2</sup>,  $\gamma_{ASA-water}$  can be calculated. The contact angle data recorded here show that even on the cast surface some spreading occurred in the beginning of the measurement ( $\approx 82^\circ$  is not the initial value). Using a contact angle of  $95^\circ$   $\gamma_{ASA-water} \approx 39$  mJ/m<sup>2</sup> is received. If one uses this value to predict interfacial contact angles of ASA in water instead of the interfacial tension value recorded earlier (Lindfors et al. 2005b), estimates of  $170^\circ$  for hydrophilic and  $25^\circ$  for hydrophobic surfaces are obtained. These match exactly with the true interfacial contact angle values that we have reported earlier (Lindfors et al. 2005b).

We also used the cast surfaces, because of their better stability, for adhesion measurements by AFM colloidal probe technique. Surface forces between glass and AKD were measured in air and in 1.0 mM NaHCO<sub>3</sub>. In air, surface force on approach was unchanged before snap-in at short separations (Fig. 17). A jump off the contact was observed, when surfaces were pulled apart. The pull-off force depended on the measuring location on the AKD surface and on the load by which the surfaces were pressed together in the contact (Fig. 18). The pull-off force increased with the load. The average of the pull-off force in all measurements was 5.3 mN/m with an average load of 5.2 mN/m.

Surface forces between glass and AKD surfaces were also measured in 1.0 mM NaHCO<sub>3</sub>, Fig. 19. The surfaces forces between approaching surfaces were repulsive. This could be most likely due to the elasticity of the surfaces. The major proportion of the repulsion is due to deformation of AKD surface (Rutland et al. 2004), and thus the range of repulsion seems to be large. An attractive pull-off force between separating surfaces was observed in some locations, but it was clearly smaller than in air.

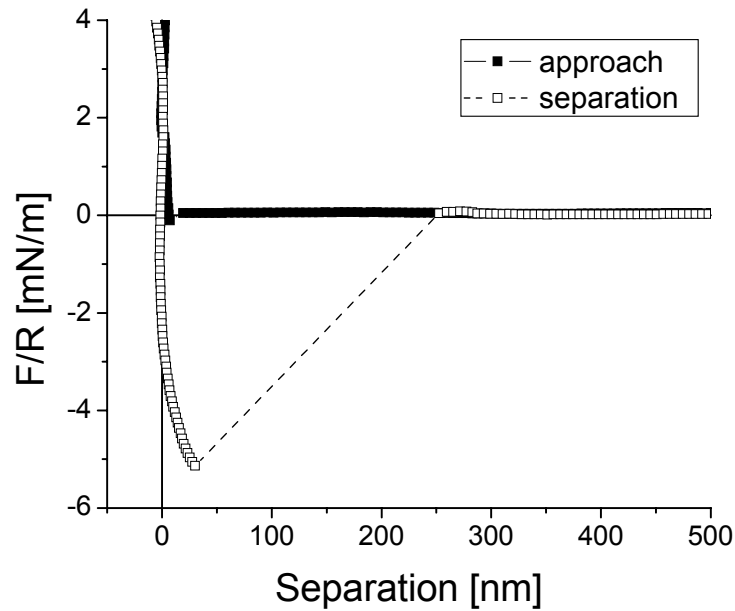


**Fig. 17.** Surface forces between glass and AKD measured in air. Filled symbols are for approaching force curve and open symbols are for separating force curve. The dotted line indicates a jump to a larger distance on separation.

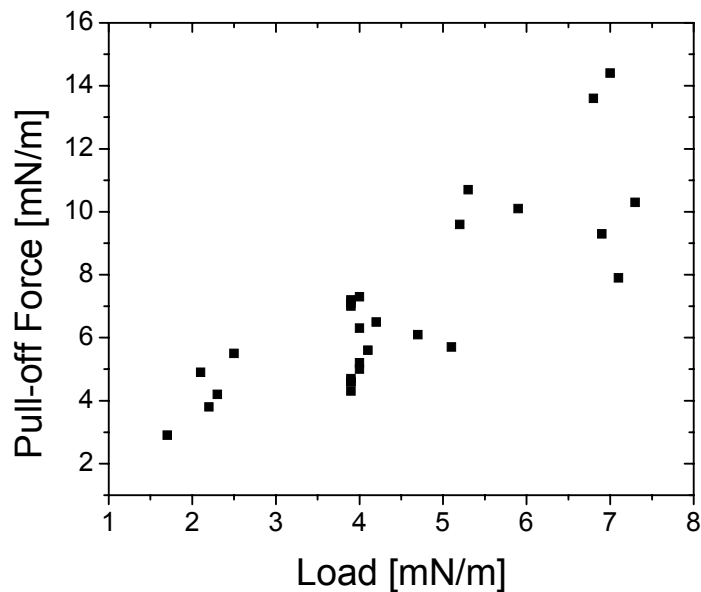


**Fig. 18.** Pull-off force of glass sphere and AKD surface as a function of load between these two. The Force is measured in air, and in one location.

A clear jump off, like the one in air, was not observed, but the surfaces remained connected at larger separations. This indicates that the surfaces were soft, and thus they stuck together. In addition, the minimum in the separation curve was not close to contact. This supported the conclusion about the deformable surface (Stiernstedt et al. 2006). The pull-off force was not systematically dependent on the load. The average of the pull-off force was 0.6 mN/m with the loads varying from 2.5 to 5.5 mN/m. The pull-off force was again dependent on the location.

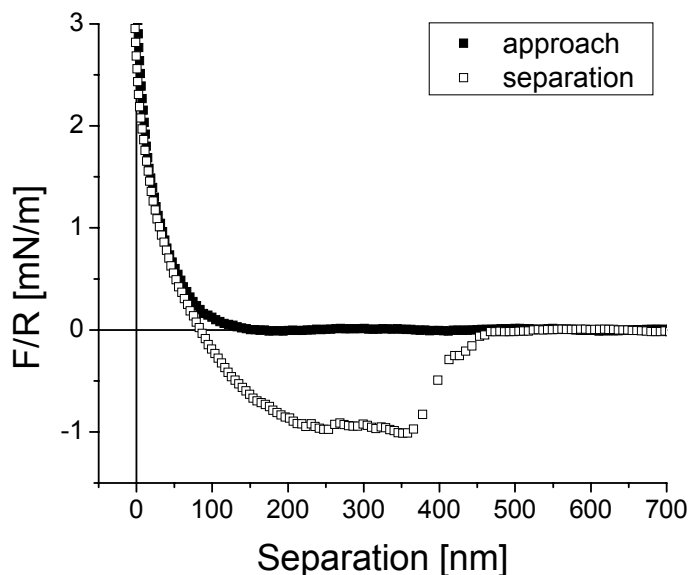


**Fig. 19.** Surface forces between glass and AKD measured in 1.0 mM NaHCO<sub>3</sub>. Filled symbols are for approaching force curve and open symbols are for separating force curve.

The surface interactions between glass and ASA in air exceeded the measuring range of the AFM, i.e. the AFM cantilever was deflected beyond the range of the detector. However, the estimated pull-off force was between 25 mN/m and 55 mN/m in air when loads were varied between -4 and 6 mN/m. An attraction was observed between approaching surfaces. Force measurements with ASA in 1.0 mM NaHCO<sub>3</sub> showed that ASA swelled and softened in solution. It was impossible to get appropriate force curves under these conditions. However, it was clear that the pull-off force was lower in solution.

## CONCLUSIONS

1. Model surfaces of AKD and ASA, suitable for variety of surface interaction measurements, were created and their feasibility for adhesion studies was demonstrated.
2. By using the created surfaces, we were also able to explain the inconsistency observed earlier in the spreading of ASA. The results obtained using the created

model surfaces verified the assumption that the hydrolysis of ASA molecules at the liquid-liquid interface is very fast and leads to erroneous interfacial tension results.

3. The molecular layer thicknesses of both AKD and ASA were found out to be ca. 2.5 nm. This knowledge can be utilized in further studies using these chemicals.
4. Force measurements with AKD and ASA with suitable corrections in experimental conditions proved that both surfaces can be used in this purpose. However, it must be recognized that surface force measurements with ASA in aqueous environment are very difficult, if not impossible. This is due to the high hydrolysis rate of ASA.

## ACKNOWLEDGMENTS

Part of this research was supported by the SHINE PRO project financed by the Finnish Funding Agency for Technology and Development (TEKES). J. Lindfors acknowledges a research grant from the Magnus Ehrnrooth foundation. Dr Leena-Sisko Johansson and Dr Joseph Campbell are gratefully acknowledged for recording the XPS data and the help in analyzing the results. Lic. Sc. Päivi Ahonen is acknowledged for performing the Ellipsometry measurements.

## REFERENCES CITED

- Alder, K., Pascher, F., and Schmitz, A. (1943). "Substituting additions. I. Addition of maleic anhydride and azodicarboxylic esters to singly unsaturated hydrocarbons. Substitution processes in the allyl position," *Berichte Der Deutschen Chemischen Gesellschaft [Abteilung] B: Abhandlungen* 76B, 27-53.
- Asakura, K., Iwamoto, M., and Isogai, A. (2006). "Influences of fatty acid anhydride components present in AKD wax on emulsion stability and paper sizing performance," *Appita J.* 59(4), 285-290.
- Bogdanovic, G., Tiberg, F., and Rutland, M. W. (2001). "Sliding friction between cellulose and silica surfaces," *Langmuir*, 17(19), 5911-5916.
- Butt, H. J. (1991). "Measuring electrostatic, Van der Waals, and hydration forces in electrolyte solutions with an atomic force microscope," *Biophys. J.* 60(6), 1438-1444.
- Davis, J. W., Roberson, W. H., and Weisgerber, C. A. (1956). "A new sizing agent for paper - Alkyl ketene dimers," *Tappi* 39(1), 21-23.
- Derjaguin, B. (1934). "Untersuchungen uber die reibung und adhesion," *Kolloid Zeit.* 69, 155-164.
- Dickson, L. E., and Berg, J. C. (2001). "The investigation of sized cellulose surfaces with scanning probe microscopy techniques," *J. Adhes. Sci. Technol.* 15(2), 171-185.
- Ducker, W. A., Senden, T. J., and Pashley, R. M. (1991). "Direct measurement of colloidal forces using an atomic force microscope," *Nature (London, United Kingdom)* 353(6341), 239-241.
- Garnier, G., Bertin, M., and Smrckova, M. (1999). "Wetting dynamics of alkyl ketene dimer on cellulosic model surfaces," *Langmuir* 15(22), 7863-7869.

- Gess, J. M. (1992). "A perspective on neutral/alkaline papermaking," *Tappi J.* 75(4), 79-81.
- Hodgson, K. T. (1994). "A review of paper sizing using alkyl ketene dimer versus alkenyl succinic anhydride," *Appita J.* 47(5), 402-406.
- Isogai, A., Morimoto, S., and Adachi, Y. (2004). "Emulsion stability and sizing performance of alkyl oleate-succinic anhydrides," *Paper Technology (Bury, United Kingdom)* 45(7), 19-24.
- Isogai, A., Taniguchi, R., and Onabe, F. (1994). "Sizing mechanism of alkyl ketene dimers. Part 4. Effects of AKD and ketone in emulsions on sizing," *Nordic Pulp & Paper Research Journal*, 9(1), 44-48.
- Isogai, A., Taniguchi, R., Onabe, F., and Usuda, M. (1992a). "Sizing mechanism of alkylketene dimers. Part 1. Possibility for AKD to form b-ketoesters in paper sheets," *Nordic Pulp & Paper Research Journal* 7(4), 193-199.
- Isogai, A., Taniguchi, R., Onabe, F., and Usuda, M. (1992b). "Sizing mechanism of alkylketene dimers. Part 2. Deterioration of alkylketene dimer emulsion," *Nordic Pulp & Paper Research Journal* 7(4), 205-211.
- Jennings, J. W., Jr., and Pallas, N. R. (1988). "An efficient method for the determination of interfacial tensions from drop profiles," *Langmuir* 4(4), 959-967.
- Johansson, L., and Campbell, J. M. (2004). "Reproducible XPS on biopolymers: Cellulose studies," *Surf. Interface Anal.* 36(8), 1018-1022.
- Lindfors, J., Ahola, S., Kallio, T., Laine, J., Stenius, P., and Danielsson, M. (2005a). "Spreading and adhesion of ASA on different surfaces present in paper machines," *Nord. Pulp Pap. Res. J.* 20(4), 453-458.
- Lindfors, J., Ylisuanto, S., Kallio, T., Laine, J., and Stenius, P. (2005b). "Spreading and adhesion of ASA on hydrophilic and hydrophobic SiO<sub>2</sub>," *Colloids and Surfaces, A: Physicochemical and Engineering Aspects* 256(2-3), 217-224.
- Lindfors, J., Laine, J., and Stenius, P. (2007) "Adhesion of hydrophobizing agents: A comparison of values determined by contact angle and JKR approach, accepted for publication in: *Contact Angle, Wettability Adhes.* 5, Mittal, K. L. (ed.).
- Mischki, T. K., Donkers, R. L., Eves, B. J., Lopinski, G. P., and Wayner, D. D. M. (2006). "Reaction of alkenes with hydrogen-terminated and photooxidized silicon surfaces. A comparison of thermal and photochemical processes," *Langmuir* 22(20), 8359-8365.
- Neimo, L. (1999). "Internal sizing of paper," *Papermaking Science and Technology*, 4, 151-203.
- Notley, S. M., Eriksson, M., Wågberg, L., Beck, S., and Gray, D. G. (2006). "Surface force measurements of spin-coated cellulose thin films with different crystallinity," *Langmuir* 22(7), 3154-3160.
- Ren, S., Yang, S., and Zhao, Y. (2003). "Micro- and macro-tribological study on a self-assembled dual-layer film," *Langmuir* 19(7), 2763-2767.
- Ren, S., Yang, S., Wang, J., Liu, W., and Zhao, Y. (2004). "Preparation and tribological studies of stearic acid self-assembled monolayers on polymer-coated silicon surface," *Chemistry of Materials* 16(3), 428-434.

- Rutland, M. W., Tyrrell, J. W. G., Attard, P. (2004). "Analysis of atomic force microscopy data for deformable materials," *J. Adhes. Sci. Technol.*, 18(10), 1199-1215.
- Stiernstedt, J., Nordgren, N., Wagberg, L., Brumer, H., Gray, D. G., Rutland, M. W. (2006). "Friction and forces between cellulose model surfaces: A comparison," *J. Colloid Interface Sci.*, 303(1), 117-123.
- Stiernstedt, J., Rutland, M. W., and Attard, P. (2005). "A novel technique for the in situ calibration and measurement of friction with the atomic force microscope," *Rev. Sci. Instrum.* 76(8), 083710/1-083710/9.
- Taniguchi, R., Isogai, A., Onabe, F., and Usuda, M. (1993). "Sizing mechanism of alkylketene dimers (AKD). Part 3. Appearance of sizing features of AKD-sized sheets," *Nordic Pulp & Paper Research Journal* 8(4), 352-357.
- Torii, A., Sasaki, M., Hane, K., and Okuma, S. (1996). "A method for determining the spring constant of cantilevers for atomic force microscopy," *Meas. Sci. Technol.* 7(2), 179-184.
- Tortonese, M., and Kirk, M. (1997). "Characterization of application specific probes for SPMs," *Proceedings of SPIE-the International Society for Optical Engineering*, 3009(Micromachining and Imaging), 53-60.
- Wurzberg, O. B., and Mazzarella, E. D. (1963). "Paper sizing," (3102064), 8.
- Zbik, M., Horn, R. G., and Shaw, N. (2006). "AFM study of paraffin wax surfaces," *Colloids and Surfaces, A: Physicochemical and Engineering Aspects* 287(1-3), 139-146.

Article submitted: Sept. 19, 2007; First round of peer-review completed: Oct. 18, 2007;  
Revised version received: Oct. 19, 2007; Article accepted and published: Oct. 20, 2007.